RSC Advances

PAPER

View Article Online
View Journal | View Issue

Check for updates

Cite this: *RSC Adv.*, 2025, **15**, 46591

Tuning collagen and collagen-alginate mechanics through extrusion bioprinting process parameters

Grace Hu,[a] Karla Gutierrez Cebrero,†[b] Nandita Venkataraman,†[c] Dharneedar Ravichandran,[c] Yunzhi Lin,[b] Zeqing Jin,[c] Zev J. Gartner[ade] and Grace X. Gu*[ac]

Bioprinting allows the fabrication of biopolymers into complex and hierarchical structures reminiscent of their organization *in vivo*. As the main structural protein found in connective tissues, type I collagen is of particular interest as a biomaterial due to its biochemical activity and ease of physical or chemical crosslinking. However, several limitations of collagen-based constructs include poor mechanical strength and inability to bear loads in dynamic conditions. Towards overcoming these challenges, this study explores the impact of higher concentration collagen bioinks (35 and 70 mg mL^{-1}) and the incorporation of an alginate hydrogel during synthesis to create designs with shape fidelity and tunable mechanical properties. Using bioprinting processes, we quantify the relationship between bioink composition, printing parameters, and post-processing on printability and mechanical behavior. Results show that both pure collagen bioinks and low-concentration collagen to alginate volume ratios of 1 : 1, 1 : 5, and 1 : 10 exhibited good printability, but increasing the alginate concentration led to greater shrinkage of scaffolds after thermo-ionic crosslinking. Uniaxial compression results indicated a directly increased modulus and compressive strength after 24 hours of crosslinking, which was also seen in tensile modulus after 12 hours of crosslinking. Notably, blend composition demonstrated the greatest influence on material stiffness, with crosslinking duration serving as a secondary factor. Scanning electron microscopy used to visualize the cross-section of these collagen constructs reveals a dense fibrous microstructure that may help reinforce mechanical properties and promote cell adhesion. Ultimately, designing collagen-based biomaterials that can be mechanically tailored through printing process parameters will inform customizable extrusion of soft tissues for regenerative medicine.

Received 3rd June 2025
Accepted 12th October 2025

DOI: 10.1039/d5ra03922c

rsc.li/rsc-advances

Introduction

The field of biomaterial additive manufacturing has catalyzed advancements in tissue engineering and regenerative medicine.[1–3] With commercialized instruments growing in availability, researchers can harness the precision and versatility of three-dimensional (3D) bioprinting to create custom tissue constructs using a wide array of materials.[4,5]

Of important initial consideration is the type of bioprinting technique utilized, as specialized methods differ in their material selection, resolution, and flexibility in pre/post-processing treatments. Extrusion-based bioprinting has been most extensively studied and involves the pneumatic or mechanical deposition of hydrogels and/or cells through a nozzle, enabling the continuous flow of bioink.[6,7] However, printing at the microscale can be limiting due to shear stresses induced by the nozzle geometry.[8,9] Meanwhile, inkjet bioprinting mainly deposits picoliter-scale droplets onto a substrate *via* thermal, piezoelectric, or electromagnetic actuation.[10–12] This technology allows for high resolution and controlled droplet delivery but typically requires the bioinks to have a low viscosity, limiting the technique's versatility. Another emerging method is vat photopolymerization-based bioprinting, which relies on light-induced crosslinking to fabricate constructs with tens of micrometer resolution. The light source, typically a laser or projector, selectively cures the resin either linearly with a scanning galvanometer for typical stereolithography (SLA) or planarly using a digital mirror to customize pixel-based optical patterns for digital light processing (DLP).[8,13] While this method can build 3D structures at fast printing speeds, its reliance on photoinitiators and UV light for curing can pose toxicity concerns that limit biomaterial options.[13,14] Extrusion-based bioprinting is therefore uniquely conducive to

---

[a] UC Berkeley-UC San Francisco Graduate Program in Bioengineering, Berkeley, CA 94720, USA. E-mail: ggu@berkeley.edu
[b] Department of Bioengineering, University of California, Berkeley, CA 94720, USA
[c] Department of Mechanical Engineering, University of California, Berkeley, CA 94720, USA
[d] Department of Pharmaceutical Chemistry, University of California, San Francisco, San Francisco, CA 94158, USA
[e] Chan Zuckerberg Biohub, San Francisco, CA 94158, USA

† These authors contributed equally.

patterning high viscosity bioinks that would otherwise be incompatible with droplet-based or vat photopolymerization methods.[6]

Bioinks are typically selected in tissue engineering applications to mimic the native extracellular matrix (ECM), which provides structural support and presents both mechanical and biochemical signals.[1] Biologically relevant hydrogels composed of proteins and/or polysaccharides are the primary materials of interest, but these soft gels with elastic moduli <100 kPa are difficult to extrude or attain shape conformity, thus requiring a support bath that may dissolve with external stimuli.[15–20]

Designing bioink formulations can be challenging due to conflicting design constraints: researchers aim to achieve robust printability while balancing material properties affecting the biology.[21,22] For example in layer-by-layer bioprinting, biomaterials must exhibit shear-thinning properties for controlled flow, sufficient viscosity to avoid structural collapse, and most importantly, excellent biocompatibility for physiological integration.[4,23] During biofabrication, printing parameters – such as nozzle diameter, extrusion rate, needle translation rate (defined in this work as print speed), and printbed temperature – can be tuned to optimize printability and minimize mechanical stress applied during extrusion.[21,24] Additionally, numerous post-processing methods are often employed to promote stable mechanical properties. For instance, popular crosslinking methods during or after printing include thermal, ionic, and photo-polymerization.[22,24] Combined with the need for materials with desirable degradation rates and mechanical properties supporting tissue repair, the resulting combinatorial design space is large and complex. As such, validating new bioink candidates may benefit from computational analytics in synergy with empirical testing.[9,25]

As the most abundant protein in connective tissues, collagen is a critical component of the ECM and plays an essential role in tissue mechanical properties as well as cell adhesion, signaling, and matrix remodeling.[26,27] The fibrillar structure of type I collagen also makes it highly effective in promoting cell migration and tissue regeneration.[28] For these and other reasons, collagen is a favorable material for bioink formulations; however, collagen's thermosensitivity, variable viscosity, and high cost present significant challenges to its adoption.[26,29] Furthermore, *in vitro* collagen bioprinting is primarily limited by poor mechanical properties, preventing the material from sustaining loads or retaining its shape after extrusion.[30,31] Previous research on collagen bioprinting mainly focuses on low concentration collagens (<5 mg mL^{-1}), leaving highly-concentrated collagens underexplored despite the fact that collagen content on average makes up 10% of the total weight in tissues (corresponding to 100 mg mL^{-1} collagen).[27,30,32] Osidak *et al.*, 2019 demonstrated direct printing of 15–40 mg mL^{-1} purified, soluble collagen ("Viscoll"), which exhibited shear-thinning behavior, good shape fidelity, and Young's moduli increasing with collagen concentration from 7.2 to 21.5 kPa.[33] The therapeutic potential of higher concentration collagens is especially promising for engineering collagen-rich tissues such as muscle and lung (35 mg mL^{-1}), colon (60 mg mL^{-1}), skin (200–400 mg mL^{-1}), and bone (250–350 mg mL^{-1}), in addition to developing better tumor models for breast cancer and more.[32,34–36]

Natural polymers such as hyaluronic acid, chitosan, gelatin, and alginate are often chosen for bioprinting due to their low cytotoxicity, mechanical tunability within the physiological range, and ability to maintain structural integrity in water.[1,37–39] Among these, alginate, a seaweed-derived linear block copolymer composed of mannuronic (M) and guluronic (G) acid units, stands out for its ease of chemical modification, biocompatibility, and biodegradation.[37,40] Pure, uncrosslinked alginate solutions behave as a low viscosity, non-Newtonian fluid without a defined geometric structure, but its gelling capability is highly tailorable *via* ionic crosslinking or the addition of thickening agents.[41] In particular, the printability and strength of alginate can be tuned by varying polymer density along with ionic crosslinking parameters, *e.g.*, Ca^{2+} ion concentration and crosslinking duration.[42] Although alginate lacks inherent bioactive properties and cell-adhesion motifs, it can significantly enhance the structural integrity and mechanical stability of pure collagen at a fraction of the cost of other additives.[43,44]

This study investigates the printability of collagen and collagen-alginate composite hydrogels, as well as their mechanical properties, in relation to printing process parameters such as polymer concentration, crosslinking duration, and infill density. At higher concentrations, collagen is denser, but the addition of alginate also results in a more viscous and gel-like bioink, making extrusion-based printing a preferable strategy. We assess the change in mechanical properties through micro-compression and tensile testing. Altogether, this work aims to inform the consistent fabrication of collagen-based scaffolds towards the overarching goal of reproducing tissue architectures in a controlled environment.

Methods

Materials

Type I bovine collagen was obtained from Advanced BioMatrix at two concentrations, a low concentration (C_L) (Lifeink 200, 35 mg mL^{-1}) and a high concentration (C_H) (Lifeink 220, 70 mg mL^{-1}). Alginate (A) (alginic acid sodium salt, medium viscosity: 15–25 cP) and calcium chloride ($CaCl_2$, anhydrous, granular, ≤7.0 mm, ≥93.0%) were purchased from Sigma-Aldrich. Phosphate-buffered saline (1× PBS, pH 7.4, Gibco) and deionized (DI) water (ASTM type II, LabChem™) were purchased from Fisher Scientific. All materials were used as received.

Preparation of collagen-alginate bioinks

Alginate (10% (w/v)) solution was first prepared by dissolving alginate powder into PBS and magnetically stirred at 1000 rpm for 2 h at room temperature. Then, the ready-to-use C_L was added to the alginate solution to form the desired volume ratio (1 : 1, 1 : 5, 1 : 10) and mechanically stirred to create a homogenous solution.

For the composite materials, 35 mg mL^{-1} collagen and 50 mg mL^{-1} alginate were combined in volume ratios of 1 : 1, 1 :

Table 1 Summary of the synthesized bioink formulations and crosslinking conditions evaluated[a]

Sample name	Sample concentration (collagen + alginate; mg mL^{-1})	Composite volume ratio	Crosslinking method	Crosslinking duration (h)
C_L	35	N/A	Thermal (37 °C)	0.5, 0.75, 12, 24
C_H	70			
C_1A_1	17.5 + 50	1 : 1	Thermo-ionic (37 °C & 50 mM $CaCl_2$)	
C_1A_5	5.83 + 83.33	1 : 5		
C_1A_{10}	3.18 + 90.83	1 : 10		

[a] Note: for the collagen-alginate composites, only C_L was used.

5, and 1 : 10 under the hypothesis that the biological benefits of collagen would complement the strength and extrudability of alginate to form viable tissue scaffolds.[44–46] Composite blends were formed with the low concentration collagen to determine if better mechanical properties could be acquired at a fraction of the cost compared to the high concentration equivalent.

Table 1 represents the nomenclature of the bioinks with respective material concentrations, crosslinking method, and crosslinking durations. Thermal crosslinking in our system predominantly stabilizes the collagen phase through fibrillogenesis and physical triple-helix re-formation, increasing network connectivity and stiffness of the collagen microstructure. The Lifeink 200/220 collagen bioinks used in this study are recommended to be crosslinked at 37 °C at 95% relative humidity, as per the manufacturer. The time of crosslinking depends on the construct size, but plateaus after complete crosslinking, and the humidity prevents denaturing of the collagen. Ionic crosslinking (Ca^{2+}-mediated) primarily acts on the alginate phase by creating egg-box junction zones that produce an ionically crosslinked alginate network. When both mechanisms are applied to the composite bioink, the two networks form an interpenetrating structure whose mechanical response depends both on (1) the relative fraction and connectivity of each polymer, as well as (2) the order and timing of crosslinking.

All prepared blends were loaded into 3 mL plastic cartridges and refrigerated until use. A solution of 50 mM $CaCl_2$ was prepared by completely dissolving $CaCl_2$ granules in deionized water at room temperature for use as an ionic crosslinking agent.

3D bioprinting and process controls

The printing process was carried out on a BioX printer (CELLINK, Sweden) using a temperature-controlled pneumatic printhead (Fig. S1a). The composite bioinks consisted of alginate in solution with dispersed collagen fibrils (Fig. 1a). Due to

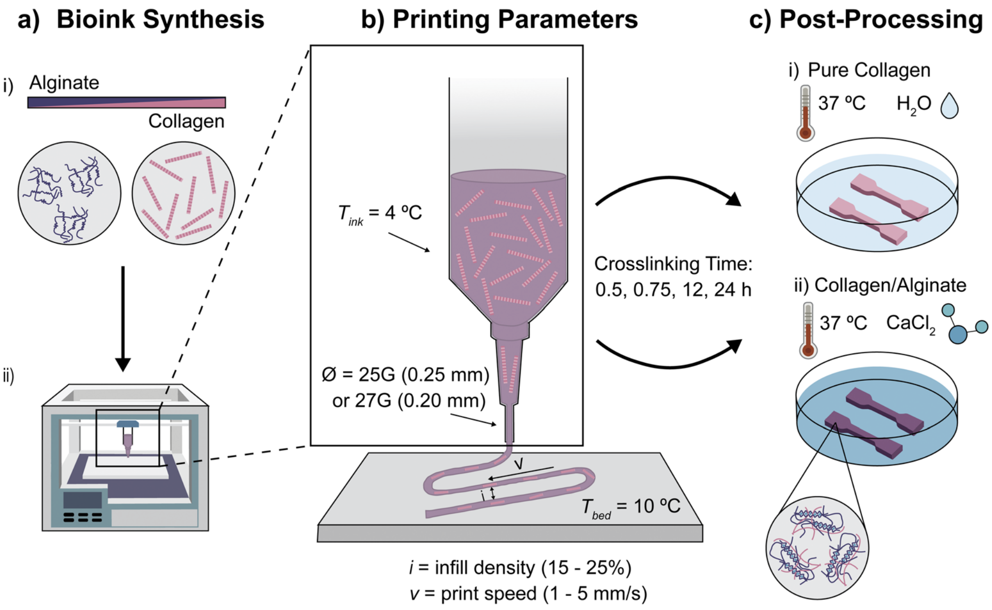

Fig. 1 Schematic overview of bioprinting stages for tunable collagen and collagen-alginate mechanical properties. (a) During bioink synthesis, the concentration and composition of collagen to alginate can be adjusted to create shear-thinning materials suitable for extrusion. (b) A variety of printing process parameters such as needle gauge (inner diameter denoted as ∅), bioink temperature (T_{ink}), printbed temperature (T_{bed}), infill density (i), and print speed (v) are controllable to optimize printability. (c) Post-fabrication treatment includes thermal crosslinking for pure collagen and both thermal and ionic crosslinking for collagen-alginate composites, where factors such as crosslinking duration and ionic strength determine final morphology and mechanical behaviors.

the thermoresponsive nature of collagen, printing was conducted under controlled temperature conditions: 4 °C for the printhead to maintain bioink viscosity, along with 10 °C for the printbed to facilitate controlled fibrillogenesis post-deposition. Temperature stabilization of both components was verified prior to loading the ink cartridge to avoid premature gelation. The cartridge was centrifuged at 800 g for 2 min at 4 °C to remove trapped air, and the minimum pressure (typically 90–200 kPa) that constant extrusion occurs was selected using the printer's inbuilt air pressure system. A blunt needle of inner diameter 25G (0.25 mm) was connected to the cartridge for continuous printing of thin filament (Fig. 1b). To ensure high-quality bioprinting, print speed was set to 1–5 mm s^{-1} according to the sample size, infill density was set to 15% and 25%, and the air gap (*i.e.*, the distance from the needle to the glass Petri dish print surface) was minimized so that the leading edge of flow was in line with the needle. Printability tests to optimize process parameters were conducted by extruding monolayered 3 × 3 grids at 100% infill density using 25G and 27G (0.20 mm) blunt needles, which were then imaged using a 2-megapixel camera toolhead. After extrusion, the pure collagen constructs underwent thermal crosslinking, while the composites were subjected to simultaneous thermal and ionic (thermo-ionic) crosslinking. At least five grids of each blend were printed and crosslinked for 24 h (Fig. 1c).

Post-crosslinking shrinkage ratio

Post-crosslinking analysis was conducted to study the effect of composition on the degree shrinkage and determine how well the samples maintained their initial dimensions. Using the same 3 × 3 grids fabricated above, all the samples were incubated at 37 °C for thermal crosslinking over 24 h inside a water bath. Pure collagen samples printed in the glass Petri dish were directly kept as is in the water bath, whereas composite samples consisting of alginate were ionically crosslinked during this heating period by immersing the grids in 50 mM $CaCl_2$.

Compression testing

Pure collagen samples of 5 × 5 × 3 mm were 3D-printed onto glass slides for compression testing since they could be crosslinked while maintaining good shape fidelity. Meanwhile, collagen-alginate composites were cut out from a larger printed sample using a razor blade to produce 5 × 5 × 3 mm cuboids due to significant shrinkage from thermo-ionic crosslinking. Samples were 3D-printed using a 25G blunt needle at 15% infill density and a constant nozzle speed of 1 mm s^{-1} rather than casting or molding bulk material specimens. Direct extrusion was chosen to obtain more accurate measures of mechanical properties imparted by the printing process at the tradeoff of achieving perfect consistency and uniformity. Samples were then transferred into Petri dishes and again crosslinked in the water bath, where pure collagen samples were crosslinked thermally with enough deionized water in the Petri dish to cover the samples, while collagen-alginate composites were crosslinked thermo-ionically with enough 50 mM $CaCl_2$ in the Petri dish to cover the samples.

Uniaxial compression testing of each hydrogel was performed using a MicroTester LT (CellScale, Canada) at a loading duration of 30 s to 10% strain with a 25 mN force transducer wire (load cell) (Fig. S1b). These static compression tests were used to determine the influence of crosslinking duration (tested after 30 min, 45 min, 12 h, and 24 h) on the compressive modulus and maximum compressive strength for each bioink composition. To calculate the initial compressive modulus (E_{comp}), the linear slope of the stress–strain curve between 5 and 10% strain was computed since it is approximately linear within the overall non-linear polymer behavior. The maximum compressive strength was taken to be the nominal stress at which the sample reaches maximum strain under test conditions. For each condition, every blend was tested with $n = 5$ samples and their average values were calculated.

Tensile testing

The influence of infill density and crosslinking duration on tensile properties was explored using uniaxial tensile testing next at 12 h and 24 h. Briefly, dogbone samples adhering to ASTM D1708 plastic microtensile specimen dimensions were 3D-printed onto glass Petri dishes using a 25G blunt needle, 15% or 25% infill density, and a constant print speed of 5 mm s^{-1}. The addition of deionized water was omitted from Petri dishes containing pure collagen dogbone samples since they were easily damaged, but 50 mM $CaCl_2$ was still needed to immerse the collagen-alginate composites within the Petri dish for ionic crosslinking.

After crosslinking, the width and thickness of each dogbone specimen were individually measured using a digital caliper before mechanical analysis. Samples were then clamped within screw grips (Type 8033, $F_{\max}$ 200 N) on a zwickiLine uniaxial tensile tester (Fig. S1c; ZwickRoell, Germany). Uniaxial stretch ($n = 5$ of each type) was performed at a strain rate of 3 mm min^{-1} until failure, where displacement and force measurements were collected and converted to stress–strain curves. Average tensile properties were represented by Young's modulus (slope of the linear region of the stress–strain curves from 5–10%) and ultimate tensile stress (stress at failure).

Scanning electron microscope (SEM) imaging

The cross-sectional region of the collagen and collagen-alginate composite dogbones post-failure was observed using a Quanta 3D field emission gun (FE)-SEM at 5 or 20 kV with a working distance of 10 mm. The structure was coated with gold-palladium using a sputter-coater for 60 s to have a coating thickness of approximately 10 nm.

Statistical analysis

Data are shown as mean ± standard deviation for five samples per experimental group. Differences between group means were assessed using a two- or three-way analysis of variance (ANOVA) for compression and tension data, respectively, with Tukey HSD post hoc test for pairwise comparisons. A $p < 0.05$ was considered statistically significant.

Results and discussion

Printability and parametric analysis

Experiments were conducted to characterize the behavior of collagen bioinks at high densities for use in 3D-bioprinting. The homogeneous C_L and C_H commercial bioinks and collagen-alginate composites (C_1A_1, C_1A_5, and C_1A_{10} with C_L) were extruded at air pressures between 90–200 kPa using 25G and 27G needles, depending on the viscosity of the hydrogel. The tests were conducted by extruding monolayered 3 × 3 grids with each line represented as a strand and imaged using the camera toolhead. The images were extracted and processed to compute dimensional data for shape fidelity of the samples pre- and post-crosslinking.

In order to evaluate the strand thickness and relative error of the print area compared to the computer-aided design (CAD), each image was analyzed using the Segment Anything Model (SAM).[47] The segmented grids were then extracted and converted to binary images. To determine the strand width, three horizontal lines and three vertical lines near the center of each row and column were measured from the binary grid image such that an average strand width was calculated from a total of 24 crossed strands per sample. The same binary processed images were used to assess the print area of each grid A_i compared to the design area A using the following equation, and a percentage of relative error was obtained from an average of at least five grids.

$$\text{Relative Error in Area (\%)} = \left[\frac{|A_i - A|}{A}\right] \times 100 \qquad (1)$$

Compared to the CAD model targeting 1 mm strand widths for the 3 × 3 grids shown in Fig. 2a, the actual prints had larger strand widths (1.33–1.73 mm) and relative error of design areas (39–70%), which is expected due to the effect of gravity on the hydrogel layer and further wetting as a result of condensation from the chilled (10 °C) printbed (Fig. 2b). Conditions such as print speed and needle gauge could also have been further optimized to promote printability, but we observed the collagen and collagen-alginate formulations then suffered greater risk of defects and nozzle clogging. The fabricated prints were imaged immediately after printing and then a day later following heating at 37 °C to allow collagen and collagen-alginate blends to crosslink in DI water or 50 mM $CaCl_2$ bath, respectively. Images taken were then labeled using SAM to extract the grid and determine the strand width and print area after applying a binary threshold (Fig. 2c–e).

While the strand width and relative error of design area listed in Table 2 were similar for each of the blends, values for the higher ratio collagen-alginate blends are slightly underestimated since grid visibility empirically decreased (Fig. S2). To reduce bias or impairment of image segmentation, a representative subset of grid samples was then manually extracted from images with the use of Canva's background removal tool. If any transparent pixels were incorrectly removed, an adjustable tip size brush could be used to manually outline the constructs pixel-by-pixel to ensure the full grid was extracted. After juxtaposing the SAM-derived masks and manually corrected masks, the difference in calculated construct area was at minimum 0.3% and maximum ~3%, suggesting that the transparency artifacts had negligible influence on the quantitative results. Upon examining structures before and after crosslinking, the pure collagen structures maintained their shape quite well (<6% shrinkage). Meanwhile, collagen-alginate blends with increasing volume ratios from 1 : 1 to 1 : 10 showed a much higher grid shrinkage from 16.36% to 39.10% (Fig. 2f and Table 2).

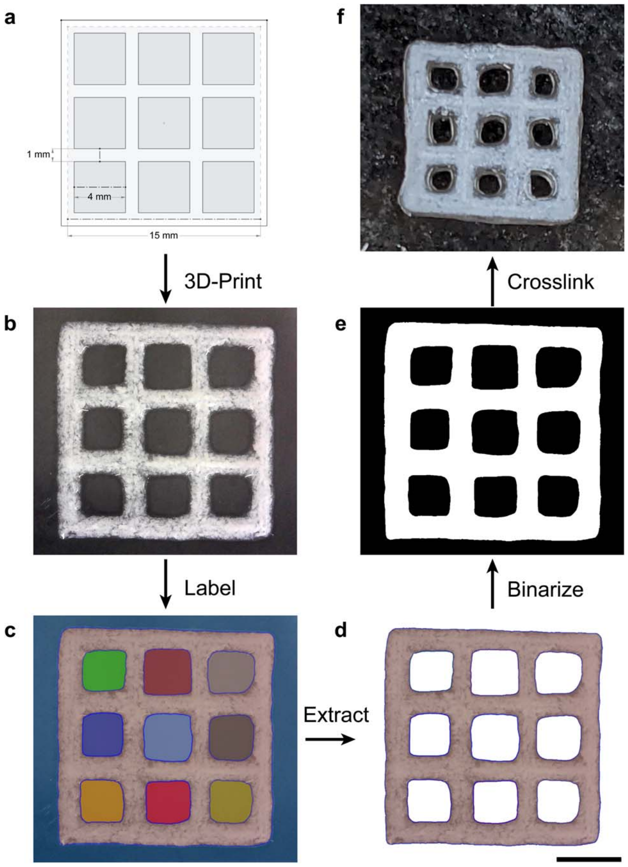

Fig. 2 Overview of printability assessment. (a) CAD model of 3 × 3 grid with 1 mm wide strands, (b) representative C_1A_1 printed sample, (c) labeled grid regions using SAM, (d) extracted hydrogel lattice, (e) binary mask of extracted lattice, and (f) slightly smaller sample post-crosslinking. Scale bar = 5 mm for all images.

Table 2 Summary of printability results for the collagen and collagen-alginate blends

Bioink	Strand width (mm)	Relative error of design area (%)	Shrinkage (%)
C_L	1.73 ± 0.14	70.03 ± 11.74	5.62 ± 4.71
C_H	1.51 ± 0.21	49.48 ± 16.60	2.71 ± 1.40
C_1A_1	1.65 ± 0.22	64.04 ± 17.91	16.36 ± 11.06
C_1A_5	1.70 ± 0.11	66.82 ± 7.52	24.90 ± 20.63
C_1A_{10}	1.33 ± 0.14	39.69 ± 5.94	39.10 ± 21.94

Compressive response

To quantify the impact of composition and crosslinking duration, micro-compression testing was performed on samples

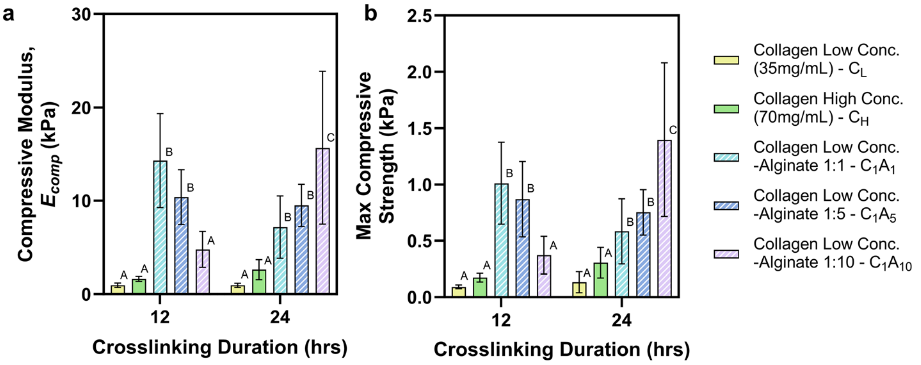

Fig. 3 Compression properties measured for collagen and collagen-alginate composites. (a) Compressive modulus and (b) max compressive strength evaluated for pure collagens (solid bar, thermally crosslinked in DI water) and collagen-alginate (dashed bar, thermo-ionically cross-linked in $CaCl_2$ solution) at increasing crosslinking durations. Different letters (A–C) by the top of each bar indicate pairwise differences, where there are significant differences between any two conditions receiving different letters ($p < 0.05$).

directly printed for pure collagen and cut out from a bulk print for collagen-alginate blends, the latter due to the significant distortion of cubes observed previously in printability tests. Samples were crosslinked for 30 min, 45 min, 12 h, and 24 h. The 30 min and 45 min crosslinking periods were insufficient to crosslink the alginate composites for compression, but data for the pure collagens can be found in Fig. S3. Compressive modulus (E_{comp}) and max compressive strength are therefore visualized for all blends at 12 h and 24 h in Fig. 3.

When comparing low (35 mg mL^{-1}) and high concentration (70 mg mL^{-1}) collagen crosslinked for the same time periods, increasing the collagen concentration increased the average stiffness linearly by approximately 2- to 3-fold ($C_{\text{L}} = 0.97$ kPa to $C_{\text{H}} = 1.63$ kPa at 12 h, $C_{\text{L}} = 0.96$ kPa to $C_{\text{H}} = 2.61$ kPa at 24 h) (Fig. 3a and S3). The compressive modulus and strength at 12 h for the collagen-alginate composites were more variable, likely due to insufficient crosslinking effects for the higher alginate compositions (Fig. 3b). With longer crosslinking duration at 24 h, the decreasing collagen to alginate volume ratios displayed increasing stiffness and strength, which can be attributed to the crosslinking effect of alginate with $CaCl_2$. When alginate, a polysaccharide with carboxylate (–COO$^-$) groups, is exposed to divalent cations such as Ca^{2+}, the Ca^{2+} exchanges with the sodium ions (Na^+) on the alginate chains. Each Ca^{2+} ion can bind to two negatively charged COO$^-$ groups and connect different alginate chains, forming an "egg-box" structure.[48,49] This ionic interaction creates a three-dimensional network, where higher temperatures for crosslinking promotes the reactivity of Ca^{2+} and transforms the alginate solution into a gel-like material with mechanical stability.[37]

The effects of crosslinking time (12 *vs.* 24 hours) and sample composition on compressive modulus and strength were evaluated using a two-way ANOVA (Table S1). While crosslinking time alone showed no major impact, sample composition significantly influenced both outputs, with the interaction between time and composition also being significant ($p < 0.001$). In a separate analysis of pure collagen samples across both short and long crosslinking durations (30 minutes to 24 hours), compressive properties were significantly affected by both crosslinking time and sample concentration ($p < 0.001$, Table S2). In essence, these results highlight composition as the primary driver of compressive behavior, with crosslinking duration playing a secondary role contingent on material composition.

Compared to previous observations, our measures of elastic moduli results lie in a comparable order of magnitude for similar type I collagen networks under compression.[50] For instance, increasing Viscoll collagen from 15 to 45 mg mL^{-1} was documented to also increase the Young's modulus of 3D-printed cubes from 7 kPa to 21 kPa, while another study increasing collagen concentration from 10–20 mg mL^{-1} reported equilibrium moduli between $\sim$10 to 30 kPa.[30,33] Furthermore, compression tests performed for 4% (w/v) alginate mixed with 3 mg mL^{-1} type 1 bovine methacrylated collagen at decreasing ratios (1 : 2, 1 : 3, or 1 : 4 collagen to alginate) showed a significant increase in compressive modulus from 31 to 143 kPa for the composites.[43] Overall, variability in results likely reflects differences in material origin, processing method, crosslinking strength, sample geometry, and infill density.

Altogether, the compressive moduli of our collagen-based hydrogel scaffolds, ranging from 0.19 to 26 kPa, are primarily suitable for soft tissue regeneration, where matching mechanical properties is essential for mechanostimulation and cell growth.[51] For instance, previous reports have demonstrated that biomaterials with similar values promoted primary neuronal cell survival ($\leq$3.8 kPa), facilitated chondrogenesis (4–32 kPa), and exhibited tunability ($\sim$10–30 kPa) for load-bearing tissues such as cartilage.[30,52–54] From our results and as expected from other studies, the composite structure is dominated more by ionic crosslinking of the alginate solution in these materials.[44]

Tensile behavior

To obtain a more complete mechanical profile and capture anisotropy for soft connective tissues, tensile tests were also performed to characterize the bond strength between printed layers and resistance to stretching. As such, 3D-printed dogbones were created at different infill density (15% or 25%) and crosslinking durations (12 h or 24 h following the compression results) before being placed under uniaxial tension to generate stress–strain curves. Pure collagen samples for all conditions were too soft and easily damaged upon transfer or gripping into the tensile fixtures. Furthermore, the maximum measured force of the collagen samples often fell below the minimum detectable force of the machine, rendering the results of the tested samples unreliable.

Thus, for the composite dogbones tested in Fig. 4a, Young's modulus (E) generally increased with greater alginate concentration across both infill densities, with values ranging from 0.56 MPa up to 1.45 MPa ($p < 0.001$; Table S1). While infill density alone did not seem to influence E, crosslinking duration and its two- and three-way interactions with infill density and composition were significant ($p < 0.05$). Meanwhile, ultimate tensile strength (UTS) displayed differences that were purely composition-dependent or only by the interaction between crosslinking duration and infill density ($p < 0.001$). Similar to results analyzed for E, UTS also increased significantly because of the independent variables' three-way interaction ($p < 0.05$, Fig. 4b). From these findings, the 25% infill density composites warrant further investigation to deduce the impact of crosslinking time on final mechanical properties.

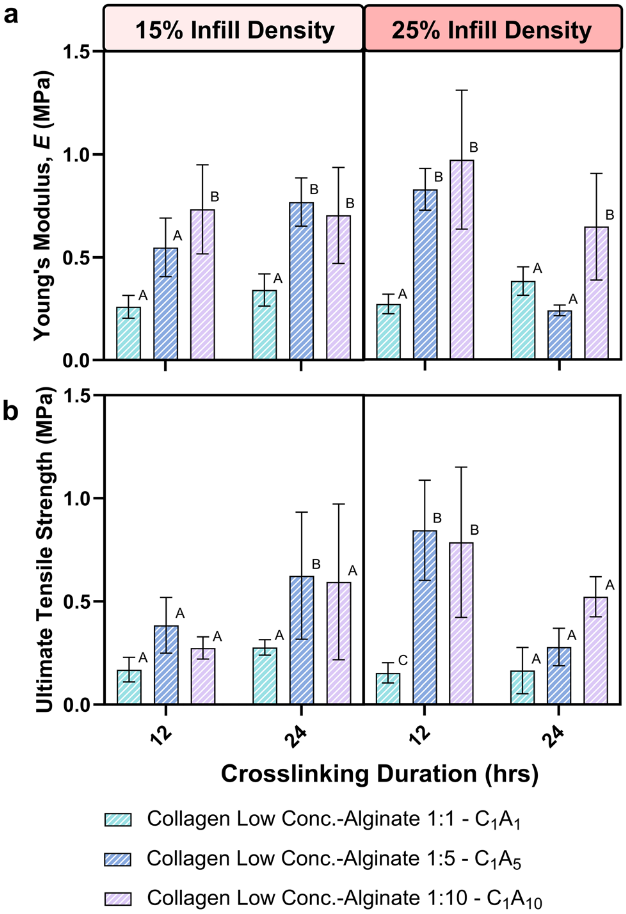

Fig. 4 Tensile properties measured for collagen-alginate composites. The effect of infill density at 15% (left) and 25% (right) was evaluated through (a) Young's modulus and (b) ultimate tensile strength measurements after 12 h and 24 h crosslinking durations. Different letters (A–C) by the top of each bar indicate pairwise differences, where there are significant differences between any two conditions receiving different letters ($p < 0.05$).

Interestingly, these values did not consistently increase for a given polymer formulation with longer crosslinking duration (from 12 h to 24 h) or between infill densities (15% to 25%). We hypothesize that this divergence might be due to competing crosslinking effects, along with significant shrinkage and distortion over long crosslinking periods. Due to variable temperature-dependent condensation, we adjusted the print-bed temperature control settings in an effort to mitigate wetting of the hydrogel structures onto the chilled glass substrate. It is also important to note that extrusion printing has been shown to align collagen fibers and is thus advantageous for improving tensile strength, while too little alginate present may compromise the structural stability of the fabricated dogbones.[28,43]

The Ca^{2+}–alginate crosslinking reaction is self-propagating, but its kinetics depend on the accessibility of the alginate's COO^- groups. Effective curing may require 12, 24, or more hours depending upon the ion concentrations. Because ion diffusion governs the process, immersion in $CaCl_2$ solution often leads to heterogeneous structures. Rapid initial crosslinking creates a dense, highly crosslinked "skin" at the surface, which then slows or blocks further diffusion into the bulk, especially for larger samples. As a result, the interior might remain less crosslinked than the outer shell, displaying variation in mechanical stability. Since the overall strength of the composite is dictated by its weakest region, longer immersion times do not necessarily resolve the diffusion limitation or improve uniformity, but prolonged crosslinking can make the samples stiffer.[55,56]

Previous experiments describing similar biomaterials highlight the vast range of tensile properties that arise from different protocols. For example, scaffolds of low molecular weight (MW) collagen (MW = 6000 or 25 000 Da) and various alginate (MW = 32 000–250 000 Da) mixtures were found to have tensile strength ranging from 0.04 MPa to approximately 2.5 MPa, which our samples fall within.[57] Another study reporting a 5 : 1 collagen-alginate scaffold observed much lower tensile strength of 50.92 kPa, which again aligns well with our results, indicating that a higher collagen concentration leads to much weaker structures.[58] Meanwhile, collagen-alginate composites tested in Zimmerling *et al.*, 2024 were relatively stronger under bulk material compression compared to our samples, whereas our tensile properties (E ∼250–1000 kPa and UTS ∼200–750 kPa) were higher than the ones they reported (E ∼25 kPa and UTS ∼6 kPa).[43] Although the infill density was approximately similar (10% *vs.* 15–25%) in this case, their usage of type 1 bovine methacrylated collagen and tensile testing methodology likely contributed to the contrasting mechanical properties. Hence, the scaffolds in our work exhibit tensile properties that build upon the repository of other soft collagen-alginate hydrogels, which vary depending on the collagen/alginate concentrations and preparation method employed.[57,59]

Morphology of hydrogels

SEM micrographs of the 3D-printed collagen and collagen-alginate scaffolds were analyzed to understand the effect of microstructure on mechanical properties. Surface imaging of

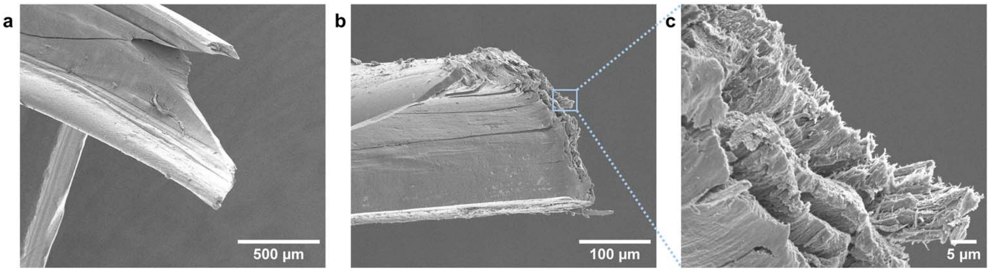

Fig. 5 SEM images of composite dogbones post-tension. Cross-sectional analysis of the failure region for collagen-alginate composition (a) 1 : 10 shows much smoother morphology at breakage compared to (b) 1 : 1 ratio where higher quantities of collagen fibers are present. (c) Inset shows higher magnification view of fibers extending from the breakage region.

the pure collagen samples revealed that the density of collagen fibers was lower in low concentration (35 mg mL^{-1}) collagen than the high concentration (70 mg mL^{-1}; Fig. S4). Notably, cross-sectional examination of collagen-alginate dogbones showed that higher alginate concentration (C_1A_{10}) led to a smoother surface of failure (Fig. 5a), whereas higher collagen concentration (C_1A_1) resulted in a more fibrous and aligned interface (Fig. 5b and c). The arrangement and distribution of collagen fibers will be crucial for cells that reconstruct their surrounding microenvironment, as well as contributing to tissue strength and flexibility.[60,61] The increase in the tensile mechanical properties as compared to compressive properties can be related to the strain alignment of collagen fibers along the extrusion direction. Under such conditions, the collagen fibers straighten even more in response to tensile forces, allowing them to bear higher loads and resist deformation effectively.[28,60,62] In contrast, collagen hydrogels behave like rigid porous solids that compress volumetrically and expel water under applied normal loads.[50]

Conclusions

Where prior studies have shown that printing concentrated collagen-based bioinks can produce mechanically improved constructs for tissue repair, this study focuses on determining how bioprinting process parameters (crosslinking duration and infill density) and compositional tuning (collagen/alginate volume ratios) can be balanced to enhance shape fidelity and mechanical properties under multiple load scenarios.[33,63,64] The results show that the constituent composition of these hydrogels can be tailored for printability and extruded shape across blends, but shrinkage issues arise with higher alginate concentrations. From our experiments, the increase in compressive and Young's modulus is more pronounced due to higher concentrations of collagen or alginate compared to crosslinking duration or infill density alone. Notably, the addition of alginate to type I collagen significantly bolsters the mechanical properties of the polymer scaffolds and expands the range of stiffnesses achievable in fabricating biocompatible hydrogels that mimic tissue ECM. Alginate is a particularly attractive material to incorporate with collagen due to its low cost of synthesis and ionic crosslinking potential, which the U.S. Food and Drug Administration (FDA) considers generally recognized as safe (GRAS) and has approved for various medical implants.[65,66] Taken together, we conclude that C_1A_1 works well for 3D bioprinting in terms of robust printability, low structural deformation post-crosslinking, cost-effectiveness, and tunable mechanical behavior. For this composition, thermo-ionic crosslinking at 12 h was sufficient at low infill densities such as 15% while maintaining the most consistent mechanical outcome.

Although a wide range of blends was investigated, more experimental data on different combinations of collagen to alginate, along with additional crosslinking durations and infill densities, may reveal a different optimized composition. Limitations of this work include sample-to-sample variation due to shrinkage and/or printing defects, as well as slight overestimation of printability due to samples becoming more transparent with alginate addition. As such, preliminary experiments backed by recent reports are underway to improve printability through pre-crosslinking methods or by directly printing into a granular microgel bath with controlled calcium ion exposure.[19,41,67–70]

As 3D bioprinting evolves alongside the advancement of modern computational tools, this experimental data may serve particularly useful in tandem with biomechanics modeling to facilitate rapid prototyping and simulations of varying collagen-alginate blends. Since the therapeutic goal of these biomaterials is to target soft tissue repair, ongoing research will further explore performance through cell viability tests, long-term stability of these ECM scaffolds before degradation, and consideration of other composite materials such as hydroxyapatite, hyaluronic acid, *etc.*[39,71] Encouragingly, previous studies have shown that *in vitro* viability within cell-laden, high-concentration collagen-based constructs remains high (generally over ∼90%) even a week after culture.[30,33,45,63,72–74] Rheological measurements also directly validate excellent printability, while biocompatibility has been shown through cell adhesion and proliferation after 3 days.[33,59,72,74] Achieving consistent biofabrication and full control of mechanical properties for these collagen-alginate composites will accelerate customizable prints, for example through gradient materials to recapitulate the hierarchical structure of connective tissues such as ligaments and tendons.[71,75] With the recent rise in engineered living materials to sustainably replace rigid materials, understanding how collagen can be architected with high stiffness and toughness may contribute towards proper bone mineralization while maintaining cell viability.[41,71,76] Ultimately, the trade-off between printability and mechanical behavior is dependent on native tissue-specific applications. Therefore, the novelty of this work in printing collagen and collagen-alginate composites with many degrees of tunability throughout the bioprinting process informs development of future bioink formulations and has promising potential for soft tissue engineering.

Author contributions

G. H. – conceptualization, methodology, formal analysis, investigation, visualization, writing – original draft preparation. K. G. C. – methodology, formal analysis, investigation, visualization, writing – original draft preparation. N. V. – methodology, formal analysis, investigation, writing – original draft preparation. D. R. – methodology, formal analysis, investigation, writing – review & editing. Y. L. – formal analysis, investigation, writing – review & editing. Z. J. – formal analysis, software. Z. J. G. – supervision, investigation, writing – review & editing. G. X. G. – conceptualization, investigation, supervision, writing – review & editing.

Conflicts of interest

The authors declare no conflicts of interest in this publication.

Data availability

All data supporting this study are included in the main article and supplementary information (SI). Supplementary information is available. See DOI: **https://doi.org/10.1039/d5ra03922c**.

Acknowledgements

This work was supported by the Barbara and Gerson Bakar Foundation (G. H., K. G. C., N. V., Y. L., Z. J., G. G.), the National Science Foundation (DMR-2323731) (G. G., Z. J.), and the National Institutes of Health (NIH) through the National Cancer Institute (NCI) Exploratory/Developmental Grant (R33CA297969) (Z. J. G.). G. H. was supported by the Bakar BioEnginuity Impact Grant and the Department of Defense (DoD) NDSEG Fellowship. Z. J. G. is an investigator in the Chan Zuckerberg Biohub San Francisco. The authors would like to acknowledge the UCSF Center for Cellular Construction (DBI-1548297) and thank the Biomolecular Nanotechnology Center (BNC) at the University of California, Berkeley for use of the SEM/FIB facilities.

References

1 S. Vanaei, M. S. Parizi, S. Vanaei, F. Salemizadehparizi and H. R. Vanaei, *Eng. Regen.*, 2021, **2**, 1–18.
2 E. S. Bishop, S. Mostafa, M. Pakvasa, H. H. Luu, M. J. Lee, J. M. Wolf, G. A. Ameer, T.-C. He and R. R. Reid, *Genes Dis.*, 2017, **4**, 185–195.
3 S. V. Murphy, P. De Coppi and A. Atala, *Nat. Biomed. Eng.*, 2019, **4**, 370–380.
4 J. Gopinathan and I. Noh, *Biomater. Res.*, 2018, **22**, 1–15.
5 R. Khoeini, H. Nosrati, A. Akbarzadeh, A. Eftekhari, T. Kavetskyy, R. Khalilov, E. Ahmadian, A. Nasibova, P. Datta, L. Roshangar, D. C. Deluca, S. Davaran, M. Cucchiarini and I. T. Ozbolat, *Adv. NanoBiomed Res.*, 2021, **1**, 1–19.
6 Y. S. Zhang, G. Haghiashtiani, T. Hübscher, D. J. Kelly, J. M. Lee, M. Lutolf, M. C. McAlpine, W. Y. Yeong, M. Zenobi-Wong and J. Malda, *Nat. Rev. Methods Primers*, 2021, **1**, 1–20.
7 H. Kim, G. Hu, A. J. Graham, G. X. Gu and Z. J. Gartner, *Cold Spring Harbor Perspect. Biol.*, 2024, **17**, 1–26.
8 K. Loukelis, N. Koutsomarkos, A. G. Mikos and M. Chatzinikolaidou, *Regener. Biomater.*, 2024, **11**, 1–34.
9 M. E. Prendergast and J. A. Burdick, *Adv. Healthcare Mater.*, 2022, **11**, 1–14.
10 H. Ravanbakhsh, V. Karamzadeh, G. Bao, L. Mongeau, D. Juncker and Y. S. Zhang, *Adv. Mater.*, 2021, **33**, 1–38.
11 G. Hu, J. Kang, L. W. T. Ng, X. Zhu, R. C. T. Howe, C. G. Jones, M. C. Hersam and T. Hasan, *Chem. Soc. Rev.*, 2018, **47**, 3265–3300.
12 H. K. Handral, V. P. Natu, T. Cao, J. Y. H. Fuh, G. Sriram and W. F. Lu, *Bio-des. Manuf.*, 2022, **5**, 396–411.
13 Y. Li, Q. Mao, K. Xu, H. Yang, Y. Huang and J. Yin, *Addit. Manuf.*, 2023, **69**, 1–13.
14 F. Liu, R. Quan, C. Vyas and E. Aslan, *Int. J. Bioprint.*, 2022, **9**, 320–335.
15 T. J. Hinton, Q. Jallerat, R. N. Palchesko, J. H. Park, M. S. Grodzicki, H.-J. Shue, M. H. Ramadan, A. R. Hudson and A. W. Feinberg, *Sci. Adv.*, 2015, **1**, 1–10.
16 K. Zhou, Y. Sun, J. Yang, H. Mao and Z. Gu, *J. Mater. Chem. B*, 2022, **10**, 1897–1907.
17 I. M. Lei, D. Zhang, W. Gu, J. Liu, Y. Zi and Y. Y. S. Huang, *Adv. Mater. Technol.*, 2023, **8**, 1–12.
18 Z. T. Xie, J. Zeng, D. H. Kang, S. Saito, S. Miyagawa, Y. Sawa and M. Matsusaki, *Adv. Healthcare Mater.*, 2023, **12**, 1–11.
19 H. Budharaju, D. Sundaramurthi and S. Sethuraman, *Bioact. Mater.*, 2024, **32**, 356–384.
20 A. Z. Nelson, B. Kundukad, W. K. Wong, S. A. Khan and P. S. Doyle, *Proc. Natl. Acad. Sci. U.S.A.*, 2020, **117**, 5671–5679.
21 C. O'Connell, J. Ren, L. Pope, Y. Zhang, A. Mohandas, R. Blanchard, S. Duchi and C. Onofrillo, in *3D Bioprinting*, ed. J. M. Crook, Springer US, New York, NY, 2020, vol. 2140, pp. 111–133.
22 N. Diamantides, L. Wang, T. Pruiksma, J. Siemiatkoski, C. Dugopolski, S. Shortkroff, S. Kennedy and L. J. Bonassar, *Biofabrication*, 2017, **9**, 1–13.
23 H. Taneja, S. M. Salodkar, A. Singh Parmar and S. Chaudhary, *J. Mol. Liq.*, 2022, **367**, 1–14.
24 Z. Jin, G. Hu, Z. Zhang, S.-Y. Yu and G. X. Gu, *Bioprinting*, 2023, **33**, 1–9.
25 B. Zheng, Z. Jin, G. Hu, J. Gu, S.-Y. Yu, J.-H. Lee and G. X. Gu, *MRS Bull.*, 2023, **48**, 1–11.
26 I. N. Amirrah, Y. Lokanathan, I. Zulkiflee, M. F. M. R. Wee, A. Motta and M. B. Fauzi, *Biomedicines*, 2022, **10**, 1–44.

27 E. O. Osidak, V. I. Kozhukhov, M. S. Osidak and S. P. Domogatsky, *Int. J. Bioprint.*, 2024, **6**, 17–26.

28 B. A. Nerger, P. T. Brun and C. M. Nelson, *Soft Matter*, 2019, **15**, 5728–5738.

29 H. Suo, J. Zhang, M. Xu and L. Wang, *Mater. Sci. Eng. C*, 2021, **123**, 1–9.

30 S. Rhee, J. L. Puetzer, B. N. Mason, C. A. Reinhart-King and L. J. Bonassar, *ACS Biomater. Sci. Eng.*, 2016, **2**, 1800–1805.

31 C. D. Morley, S. T. Ellison, T. Bhattacharjee, C. S. O'Bryan, Y. Zhang, K. F. Smith, C. P. Kabb, M. Sebastian, G. L. Moore, K. D. Schulze, S. Niemi, W. G. Sawyer, D. D. Tran, D. A. Mitchell, B. S. Sumerlin, C. T. Flores and T. E. Angelini, *Nat. Commun.*, 2019, **10**, 1–9.

32 E. E. Antoine, P. P. Vlachos and M. N. Rylander, *Tissue Eng. B Rev.*, 2014, **20**, 683–696.

33 E. O. Osidak, P. A. Karalkin, M. S. Osidak, V. A. Parfenov, D. E. Sivogrivov, F. D. A. S. Pereira, A. A. Gryadunova, E. V. Koudan, Y. D. Khesuani, V. A. Kasyanov, S. I. Belousov, S. V. Krasheninnikov, T. E. Grigoriev, S. N. Chvalun, E. A. Bulanova, V. A. Mironov and S. P. Domogatsky, *J. Mater. Sci.: Mater. Med.*, 2019, **30**, 1–12.

34 K. Tarnutzer, D. Siva Sankar, J. Dengjel and C. Y. Ewald, *Sci. Rep.*, 2023, **13**, 1–12.

35 T. J. McKee, G. Perlman, M. Morris and S. V. Komarova, *Sci. Rep.*, 2019, **9**, 1–15.

36 W. Shi, S. Mirza, M. Kuss, B. Liu, A. Hartin, S. Wan, Y. Kong, B. Mohapatra, M. Krishnan, H. Band, V. Band and B. Duan, *Adv. Healthcare Mater.*, 2023, **12**, 1–16.

37 M. D. Giuseppe, N. Law, B. Webb, R. A. Macrae, L. J. Liew, T. B. Sercombe, R. J. Dilley and B. J. Doyle, *J. Mech. Behav. Biomed. Mater.*, 2018, **79**, 150–157.

38 J.-H. Shim, K.-M. Jang, S. K. Hahn, J. Y. Park, H. Jung, K. Oh, K. M. Park, J. Yeom, S. H. Park, S. W. Kim, J. H. Wang, K. Kim and D.-W. Cho, *Biofabrication*, 2016, **8**, 1–12.

39 Q. Xu, J. E. Torres, M. Hakim, P. M. Babiak, P. Pal, C. M. Battistoni, M. Nguyen, A. Panitch, L. Solorio and J. C. Liu, *Mater. Sci. Eng. R Rep.*, 2021, **146**, 1–35.

40 R. Abka-khajouei, L. Tounsi, N. Shahabi, A. K. Patel, S. Abdelkafi and P. Michaud, *Mar. Drugs*, 2022, **20**, 1–18.

41 T. Gonzalez-Fernandez, A. J. Tenorio, K. T. Campbell, E. A. Silva and J. K. Leach, *Tissue Eng., Part A*, 2021, **27**, 1168–1181.

42 A. A. Aldana, F. Valente, R. Dilley and B. Doyle, *Bioprinting*, 2021, **21**, 1–9.

43 A. Zimmerling, Y. Zhou and X. Chen, *J. Funct. Biomater.*, 2024, **15**, 1–14.

44 Y. Chen, Y. Zhou and C. Wang, *J. Compos. Sci.*, 2022, **6**, 1–12.

45 X. Yang, Z. Lu, H. Wu, W. Li, L. Zheng and J. Zhao, *Mater. Sci. Eng. C*, 2018, **83**, 195–201.

46 T. Hu and A. C. Y. Lo, *Polymers*, 2021, **13**, 1–26.

47 A. Kirillov, E. Mintun, N. Ravi, H. Mao, C. Rolland, L. Gustafson, T. Xiao, S. Whitehead, A. C. Berg, W.-Y. Lo, P. Dollár and R. Girshick, *2023 IEEE/CVF International Conference on Computer Vision (ICCV)*, 2023.

48 K. A. Bowman, O. A. Aarstad, M. Nakamura, B. T. Stokke, G. Skjåk-Bræk and A. N. Round, *Carbohydr. Polym.*, 2016, **148**, 52–60.

49 I. Donati and B. E. Christensen, *Carbohydr. Polym.*, 2023, **321**, 1–17.

50 C. S. O'Bryan, Y. Ni, C. R. Taylor, T. E. Angelini and K. D. Schulze, *Langmuir*, 2024, **40**, 4228–4235.

51 D. Goder Orbach, I. Roitman, G. Coster Kimhi and M. Zilberman, *Polymers*, 2024, **16**, 1–16.

52 N. Naseri, J.-M. Poirier, L. Girandon, M. Fröhlich, K. Oksman and A. P. Mathew, *RSC Adv.*, 2016, **6**, 5999–6007.

53 E. Schuh, J. Kramer, J. Rohwedel, H. Notbohm, R. Müller, T. Gutsmann and N. Rotter, *Tissue Eng., Part A*, 2010, **16**, 1281–1290.

54 E. R. Aurand, K. J. Lampe and K. B. Bjugstad, *Neurosci. Res.*, 2012, **72**, 199–213.

55 C. K. Kuo and P. X. Ma, *Biomaterials*, 2001, **22**, 511–521.

56 H. Malektaj, A. D. Drozdov and J. deClaville Christiansen, *Polymers*, 2023, **15**, 1–11.

57 T. C. Ho, J.-S. Park, S.-Y. Kim, H. Lee, J.-S. Lim, S.-J. Kim, M.-H. Choi, S. Y. Nam and B.-S. Chun, *Mar. Drugs*, 2021, **19**, 1–16.

58 L. Sun, Y. Shen, M. Li, Q. Wang, R. Li and S. Gong, *Polymers*, 2024, **16**, 1–12.

59 G. Kim, S. Ahn, Y. Kim, Y. Cho and W. Chun, *J. Mater. Chem.*, 2011, **21**, 6165–6172.

60 M. Sharabi, *Front. Mater.*, 2022, **8**, 1–28.

61 B. M. Baker, B. Trappmann, W. Y. Wang, M. S. Sakar, I. L. Kim, V. B. Shenoy, J. A. Burdick and C. S. Chen, *Nat. Mater.*, 2015, **14**, 1262–1268.

62 M. Witte, M. Rübhausen, S. Jaspers, H. Wenck and F. Fischer, *Sci. Rep.*, 2021, **11**, 1–8.

63 E. E. Beketov, E. V. Isaeva, N. D. Yakovleva, G. A. Demyashkin, N. V. Arguchinskaya, A. A. Kisel, T. S. Lagoda, E. P. Malakhov, V. I. Kharlov, E. O. Osidak, S. P. Domogatsky, S. A. Ivanov, P. V. Shegay and A. D. Kaprin, *Int. J. Mol. Sci.*, 2021, **22**, 1–13.

64 N. V. Arguchinskaya, E. E. Beketov, A. A. Kisel, E. V. Isaeva, E. O. Osidak, S. P. Domogatsky, N. V. Mikhailovsky, F. E. Sevryukov, N. K. Silantyeva, T. A. Agababyan, S. A. Ivanov, P. V. Shegay and A. D. Kaprin, *Int. J. Bioprint.*, 2021, **7**, 104–113.

65 G. Cattelan, A. Guerrero Gerbolés, R. Foresti, P. P. Pramstaller, A. Rossini, M. Miragoli and C. Caffarra Malvezzi, *Front. Bioeng. Biotechnol.*, 2020, **8**, 1–16.

66 N. Myung, S. Hwang, W. Ha and H. W. Kang, *Adv. Therapeut.*, 2024, **7**, 1–14.

67 J. Hazur, R. Detsch, E. Karakaya, J. Kaschta, J. Teßmar, D. Schneidereit, O. Friedrich, D. W. Schubert and A. R. Boccaccini, *Biofabrication*, 2020, **12**, 1–16.

68 H. Budharaju, D. Sundaramurthi and S. Sethuraman, *Biomater. Adv.*, 2023, **152**, 1–17.

69 A. Lee, A. R. Hudson, D. J. Shiwarski, J. W. Tashman, T. J. Hinton, S. Yerneni, J. M. Bliley, P. G. Campbell and A. W. Feinberg, *Science*, 2019, **365**, 482–487.

70 L. G. Brunel, F. Christakopoulos, D. Kilian, B. Cai, S. M. Hull, D. Myung and S. C. Heilshorn, *Adv. Healthcare Mater.*, 2024, **13**, 1–12.

71 T. Lei, T. Zhang, W. Ju, X. Chen, B. C. Heng, W. Shen and Z. Yin, *Bioact. Mater.*, 2021, **6**, 2491–2510.

72 E. O. Osidak, E. P. Kalabusheva, E. V. Alpeeva, S. I. Belousov, S. V. Krasheninnikov, T. E. Grigoriev, S. P. Domogatsky, E. A. Vorotelyak and E. S. Chermnykh, *Materialia*, 2021, **20**, 1–11.

73 E. V. Isaeva, E. E. Beketov, V. V. Yuzhakov, N. V. Arguchinskaya, A. A. Kisel, E. P. Malakhov, T. S. Lagoda, N. D. Yakovleva, P. V. Shegai, S. A. Ivanov and A. D. Kaprin, *Cell Tiss. Biol.*, 2021, **15**, 493–502.

74 Y. Song, S. Hua, S. Sayyar, Z. Chen, J. Chung, X. Liu, Z. Yue, C. Angus, B. Filippi, S. Beirne, G. Wallace, G. Sutton and J. You, *Bioprinting*, 2022, **28**, 1–13.

75 Y. Maghdouri-White, N. Sori, S. Petrova, H. Wriggers, N. Kemper, A. Dasgupta, K. Coughenour, S. Polk, N. Thayer, R. D. Mario, B. Simon Dpm, A. Bulysheva, K. Bonner, S. Arnoczky Dvm, S. Adams and M. P. Francis, *Biomed. Mater.*, 2021, **16**, 1–21.

76 C. M. Heveran, R. Gerlach, C. J. Hernandez, K. Intemann, A. S. Meyer, C. Ajo-Franklin, M. Charrier, W. V. S. III, N. Joshi, A. Nelson and M. W. Fields, *Matter*, 2024, **7**, 2846–2858.